Direction of Force Generated by the Inner Row of Dynein Arms on Flagellar Microtubules

Laura A. Fox and Winfield S. Sale

Department of Anatomy and Cell Biology, Emory University School of Medicine, Atlanta, Georgia 30322

Abstract. Our goal was to determine the direction of force generation of the inner dynein arms in flagellar axonemes. We developed an efficient means of extracting the outer row of dynein arms in demembranated sperm tail axonemes, leaving the inner row of dynein arms structurally and functionally intact. Sperm tail axonemes depleted of outer arms beat at half the beat frequency of sperm tails with intact arms over a wide range of ATP concentrations. The isolated, outer arm–depleted axonemes were induced to undergo microtubule sliding in the presence of ATP and trypsin. Electron microscopic analysis of the relative direction of microtubule sliding (see Sale, W. S. and P. Satir, 1977, *Proc. Natl. Acad. Sci. USA*, 74:2045–2049) revealed that the doublet microtubule with the row of inner dynein arms, doublet N, always moved by sliding toward the proximal end of the axoneme relative to doublet N+1. Therefore, the inner arms generate force such that doublet N pushes doublet N+1 tipward. This is the same direction of microtubule sliding induced by ATP and trypsin in axonemes having both inner and outer dynein arms. The implications of this result for the mechanism of ciliary bending and utility in functional definition of cytoplasmic dyneins are discussed.

MICROTUBULES are involved in a variety of motile processes in eukaryotic cells, such as directed intracellular transport of organelles (2, 41, 42), directed movement of chromosomes (19, 23), and oscillatory bending of cilia and flagella (12, 40). An understanding of the mechanism of these motile processes has depended upon the recognition that microtubules have inherent structural polarity (7) and that each motile event requires an ATPase-mechanochemical translocator, or motor, to generate directed sliding movements along microtubule tracks.

Apparently each microtubule-associated motor generates force in only a single direction with respect to the intrinsic structure of the microtubule it moves along. For example, in ciliary axonemes the inner and outer dynein arms on microtubule N, the doublet microtubule with the arms attached, generate a net force such that microtubule N moves toward the minus or proximal end of microtubule N+1 (38). (The plus end of microtubules is defined as the end that is equivalent, based upon inherent structural polarity, to the distal end of microtubules in ciliary and flagellar axonemes [7].) Another microtubule-associated motor, kinesin, has been isolated and characterized (43, 50) based, in part, upon technical advances (1) and development of functional assays (15, 52). As opposed to the paired dynein arms, kinesin generates movement only toward the plus end of the microtubule it moves along; relative to kinesin, the microtubule moves toward its own minus end (51). Other microtubule-associated translocators have been identified in neurons (4, 14, 27, 51) and other cell types (26, 36), but have not yet been completely characterized, and may have properties distinct from dynein or kinesin.

From these and other results it has been hypothesized that bidirectional transport on cytoplasmic microtubules results from two different classes of motors that generate force in opposite directions. One class is kinesin-like and moves toward the plus ends of microtubule tracks and the other class is dynein-like and moves toward the minus ends of microtubule tracks (51). However, these conclusions about the polarity of dynein-based microtubule sliding assume that both inner and outer arms are equivalent in activity and generate force with the same polarity. The question remains whether each row of arms is equivalent in mechanism. Since the inner dynein arms differ from the outer arms in composition (6, 16, 22, 30, 34), solubility (3, 13), structure (17, 18), and possibly function (6), it is necessary to determine the polarity of force of the inner and outer rows of dynein arms independent of each other.

We have developed an efficient means of removing the outer row of dynein arms from sea urchin sperm tail axonemes under conditions that leave the inner row of arms intact and functional. We have found that the inner row of dynein arms generates force in a single direction such that the dynein arms of doublet N push doublet N+1 toward the tip. Therefore, inner dynein arms move toward the minus end of microtubule N+1. This is opposite the direction that kinesin moves along microtubules. These methods and results offer a new and generally available opportunity to study functional re-

Portions of this work were presented at the 31st Annual Meeting of the Biophysical Society (Sale, W. S., and L. A. Fox, 1987, *Biophys. J.*, 51[2, pt 2]:213a).

constitution of outer dynein arm components (10) and to investigate the composition, mechanism, and regulation of the inner dynein arms.

Materials and Methods

Materials

Sperm cells from the sea urchin *Lytechinus pictus* were used. Animals were injected with 0.53 M KCl and semen was collected and stored undiluted on ice for <1 d. ATP was from Boehringer Mannheim Biochemicals (Indianapolis, IN). Trypsin was from Worthington (trypsin-TPCK; Cooper Biomedical Inc., Malvern, PA). Elastase was chromatographically pure (EO127; Sigma Chemical Co., St. Louis, MO). All other chemicals were from Sigma Chemical Co.

Demembranation and Reactivation of Motility

For demembranation and outer arm extraction, 15 μL of undiluted semen was suspended in 0.5 ml buffer containing 0.6 M KCl, 10 mM Tris, 2.0 mM EGTA, 1.0 mM $MgSO_4$, 1.0 mM dithiothreitol (DTT), 0.05% Triton X-100, and 50 μM cAMP. For comparison, outer arm intact samples were prepared by demembranation in the same buffer with 0.15 M KCl. After 3 min at room temperature, a 20-μL aliquot of the demembranated sperm cells was added to 2.5 ml of reactivation buffer comprised of 10 mM Tris, pH 8.15, 0.25 M potassium acetate, 2.0 mM $MgSO_4$, 1.0 mM DTT, 0.1 mM EGTA, and variable ATP. Percent motility, waveforms, and beat frequency were assessed using stroboscopic darkfield light microscopy (5). A crucial factor in our successful reactivation of outer arm–depleted axonemes was the use of 0.25 M potassium acetate in the reactivation buffer (see reference 11). In contrast to outer arm intact axonemes that were 100% motile in reactivation buffers containing a wide range of potassium acetate (75 mM–0.3 M), outer arm–depleted axonemes were mostly quiescent in reactivation buffer containing <1 0.15 M potassium acetate. Outer arm–depleted axonemes were 100% motile in reactivation buffer made with >0.2 M potassium acetate. Therefore, we routinely used 0.25 M potassium acetate. Preliminary studies revealed that beat frequency of intact axonemes, at 0.1 mM ATP, was unaffected by changes in potassium acetate concentration. Therefore, the basis for the differential effect of potassium acetate concentration on successful reactivation of intact versus outer arm–depleted axonemes may be a regulatory mechanism not directly linked to beat frequency. Beat frequency was a reliable assay of the extraction of outer arms, since such outer arm–depleted axonemes beat at exactly half the beat frequency of axonemes with intact outer arms demembranated in the presence of 0.15 M KCl (see Results). Outer arm extraction was also assessed by electron microscopy, gel electrophoresis, and immunostaining as described below.

For elastase-induced microtubule sliding disruption and measurements of sliding rates, demembranated cells were suspended in reactivation buffer that contained 0.4 mM $CaCl_2$ and 1 mM ATP. Quiescent sperm tail axonemes (see reference 37) were applied to a glass slide, a coverslip was added, and elastase (20 μg/ml) in the same reactivation buffer was slowly drawn across the slide. Microtubule sliding was recorded on videotape, and microtubule sliding rates were determined as described previously (37).

Axoneme Isolation and ATP, Trypsin-induced Microtubule Sliding

For axoneme isolation and study of the direction of microtubule sliding, sperm cells were demembranated as described above in either 0.15 or 0.6 M KCl demembranation buffer. After 3 min, a 0.2-ml aliquot was added to 2.5 ml of reactivation buffer that contained no added ATP, and the sample was homogenized with 1 pass in a 5-ml motor-driven Teflon homogenizer to separate sperm heads from tails and fracture axonemes. Another 0.2-ml aliquot of the same demembranated sperm sample was suspended in reactivation buffer containing 0.1 mM ATP, and beat frequency was measured by stroboscopic darkfield microscopy. As described above, beat frequency was a reliable assay of outer arm extraction, since sperm tail axonemes extracted in 0.6 M KCl always beat at half the frequency of axonemes extracted in 0.15 M KCl.

Microtubule sliding of outer arm–depleted axonemes was induced by the addition of reactivation buffer containing 0.1 mM ATP and 25 μg/ml trypsin. For these experiments trypsin was used because it routinely resulted in ATP-induced microtubule sliding. We have not examined the effects of elastase in this type of experiment. For light microscopic observations of microtubule sliding, fractured axoneme samples were applied to a glass slide and a coverslip was added. The ATP and trypsin-containing reactivation buffer was added to one edge of the coverslip and the solution was drawn across the slide by applying absorbant strips of lens paper to the opposite edge of the cover slip. All observations made use of the Zeiss Ultra darkfield condenser.

For whole-mount electron microscopy, fractured axonemes were applied to Formvar/carbon-coated, polylysine-treated grids (38). The grids were gently rinsed with reactivation buffer and floated on a drop of ATP-trypsin containing reactivation buffer for 5 or 10 s. The grids were transferred to reactivation buffer devoid of ATP and containing 1.0 mg/ml soybean trypsin inhibitor. After 30 s the grids were transferred to a drop of 0.1% glutaraldehyde in the same reactivation buffer, rinsed with several drops of 1% aqueous uranyl acetate, and air-dried. With this procedure there were typically one to four axonemal fragments per 300-mesh grid square. Control specimens were treated as above, but in either buffer alone, ATP alone, or trypsin alone.

Miscellaneous Procedures

For thin-section electron microscopy, demembranated sperm samples were pelleted at 9,000 *g* for 10 min and fixed in 1% glutaraldehyde and 1% tannic acid in 0.1 M sodium cacodylate buffer, pH 7.3. Samples were processed and sectioned as described previously (37). Micrographs of randomly selected transverse sections were taken at 25,000×, and the presence or absence of outer and inner arms were scored.

For gel electrophoresis, specimens were prepared in the sample buffer described in Tang et al., (47). High molecular weight polypeptides were separated by SDS-PAGE in a 3–6% linear acrylamide gradient and with a linear 0–8-M urea gradient as described in Piperno and Luck (33).

For immunoblots, high molecular weight polypeptides were electrophoretically transferred to nitrocellulose (49). The transfer buffer contained 50 mM Tris-base, 384 mM glycine, 0.017% SDS, and 20% methanol. After transfer, nitrocellulose strips were incubated in PBS, 3% BSA, and 0.05% Tween-20 before immunostaining. Harvest fluid containing mouse monoclonal antibody C-241-2, an antibody to the β heavy chain of outer dynein arms from sea urchin sperm tails (kindly provided by G. Piperno, The Rockefeller University, New York; see reference 32) was diluted 10–20-fold in PBS-BSA and used for staining. Antibody staining was detected using a two-step biotinylated anti-mouse, streptavidin–horseradish peroxidase system. Biotinylated anti-mouse (RPN1061; Amersham Corp., Arlington Heights, IL) and streptavidin–horseradish peroxidase (RPN1051; Amersham Corp.) were diluted 400-fold in PBS-BSA before use. Antibody complexes were detected by development with 0.5 mg/ml diaminobenzidine and 8.5 μL 30% hydrogen peroxidase in 50 ml PBS.

Results

Outer Dynein Arm Extraction

Analysis of cross sections of demembranated sperm showed that 0.15 M KCl demembranation buffer leaves 100% of both the inner and outer rows of dynein arms intact (n = 103 axonemes). The 0.6 M KCl demembranation buffer completely removed the outer row of arms but left the inner row of arms 97% intact (n = 102 axonemes). Using the α and β heavy chains (see reference 47) of the outer dynein arm as a standard, gel electrophoresis revealed that the outer arm proteins were retained in the axonemal pellet for samples extracted in the 0.15 M KCl buffer (Fig. 1 *a*), whereas 0.6 M KCl completely solubilized the outer arm heavy chains (Fig. 1 *b*, *arrows*). Presumably, the dynein high molecular weight polypeptides that remained in extracted axonemes were associated with the inner row of dynein arms. To verify that the outer dynein arms were completely extracted in the 0.6 M KCl buffer, the proteins were transferred to nitrocellulose for immunoblot analysis using a mouse monoclonal monospecific antibody to the β heavy chain of the outer dynein arms (see Materials and Methods). Fig. 2 (*left*) shows the Coomas-

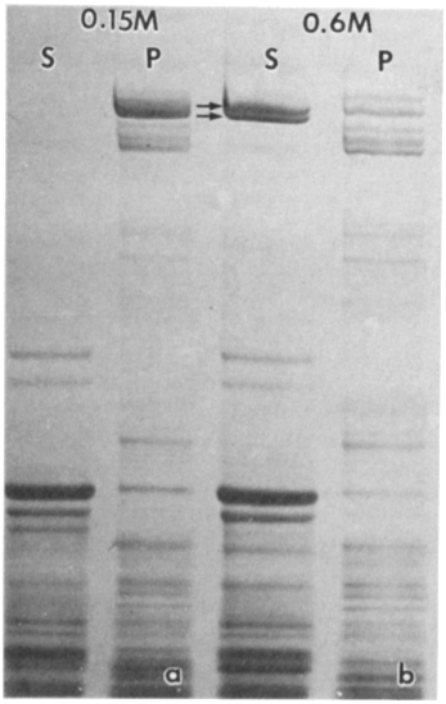

Figure 1. (*a*) SDS-PAGE of the axonemal pellet (lane *P*) and detergent supernatant (lane *S*) of sperm tail axonemes demembranated in the presence of 0.15 M KCl, and (*b*) the axonemal pellet (lane *P*) and detergent supernatant (lane *S*) of sperm tail axonemes demembranated in the presence of 0.6 M KCl. The α and β heavy chains of the outer dynein arms (*arrows*) were extracted in 0.6 M KCl but remained with the axonemes in 0.15 M KCl. The high molecular weight polypeptides that remained after outer arm removal are presumably associated with inner dynein arm structures. One of these bands approximately comigrates with the α heavy chain of the outer arm.

sie Blue-stained polypeptides of axonemes (lane *a*), high salt extract (lane *b*), and overloaded extracted axonemes (lane *c*). Fig. 2 (*right*) is the immunoblot of a nitrocellulose replica of the same proteins shown at left. The antibody only stained the axonemes (lane *a'*) and high salt extract (lane *b'*). The extracted axonemes were completely devoid of the antigen (lane *c'*). This same result was found over a wide range of

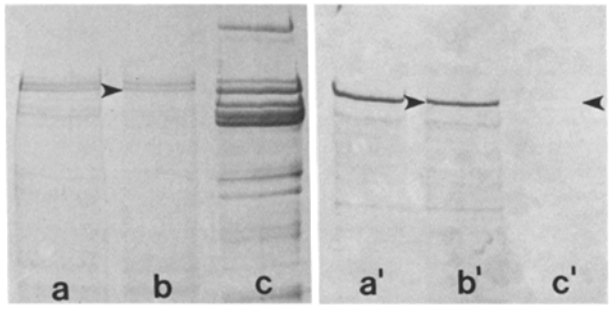

Figure 2. (*Left*) The Coomassie Blue-stained proteins of 25-μg axonemes (lane *a*), 20 μg 0.6-M KCl extract (lane *b*), and 150 μg 0.6-M KCl-extracted axonemes (lane *c*). Lanes *a'*, *b'*, and *c'* at right are the corresponding nitrocellulose replicas immunostained with a mouse monoclonal antibody, C-241-2, specific for the β heavy chain of the outer dynein arm. The β heavy chain was completely devoid in the extracted axonemes (lane *c'*).

Table I. Comparison of Beat Frequencies of Intact vs. Outer Arm-depleted Sperm Tails

ATP	Intact	Outer arm-depleted	Ratio of intact beat frequencies/outer arm-depleted beat frequencies
mM	*Hz (±SD)*	*Hz (±SD)*	
0.500	24.6 (±1.0)	11.1 (±0.65)	2.22
0.100	17.0 (±1.0)	8.3 (±0.55)	2.05
0.050	10.8 (±1.0)	5.8 (±0.46)	1.86
0.025	6.0 (±0.5)	3.4 (±0.51)	1.76

Cells were demembranated in 0.15 M KCl for intact and 0.6 M KCl for outer arm-depleted sperm tails and reactivated as described in Materials and Methods. Beat frequencies were measured stroboscopically under darkfield illumination. Intact specimens were directly compared with outer arm-depleted specimens for each ATP concentration. Beat frequencies listed are the mean values from three different experiments in which 10 individual sperm were counted for each sample.

protein loads from 20 to 150 μg. From these results we were confident that the 0.6 M KCl demembranation buffer efficiently removed the outer arms.

Reactivation of Motility and Microtubule Sliding Rates

The outer arm-depleted sperm tail axonemes could be reactivated to beat by addition of ATP (9). Outer arm-depleted axonemes exhibited waveforms that were similar to those of intact outer arm axonemes. The primary difference is that outer arm-depleted sperm tails move at half the beat frequency of the control axonemes over a wide range of ATP concentrations (Table I). Therefore, for every sample studied, we routinely measured beat frequency in 0.1 mM ATP to assess the successful extraction of outer arms.

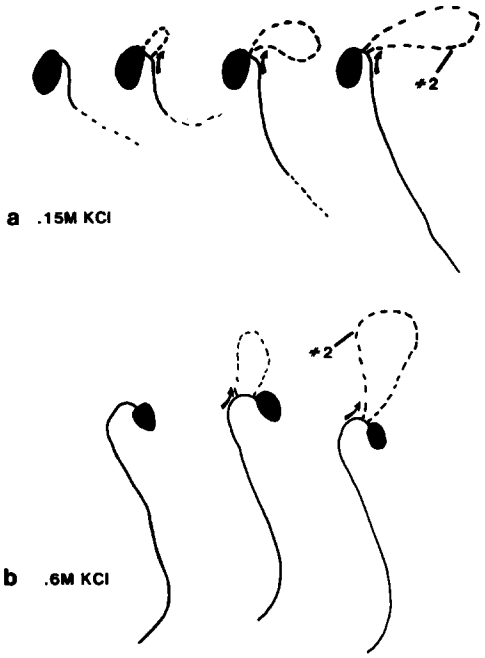

Figure 3. Traces from selected video fields illustrating the pattern of elastase-induced microtubule sliding in calcium/ATP-induced stationary bends for sperm tail axonemes with intact (*a*) and outer arm-depleted (*b*) dynein arms. In each case subset 2 slides proximally (*arrows*) relative to subset 1.

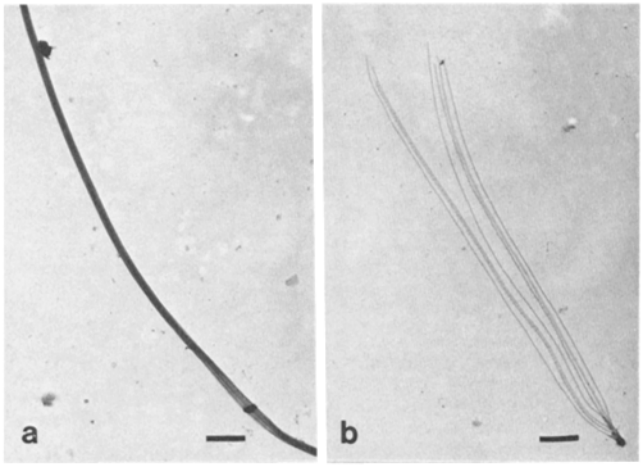

Figure 4. Examples of (*a*) an intact axoneme and (*b*) a splayed axoneme stained with uranyl acetate and examined by electron microscopy. Bar, 10 μm.

Both the intact and outer arm–depleted sperm tails could be induced to form stationary basal, principal bends in reactivation buffer that contained 0.4 mM $CaCl_2$ and 1 mM ATP (see reference 37). Addition of elastase to the calcium/ATP-induced quiescent axonemes resulted in microtubule sliding disruption as described earlier (Fig. 3, reference 37). The pattern of microtubule sliding is illustrated in the traces from selected video fields for both sperm tails with intact outer dynein arms (Fig. 3 *a*) and outer arm–depleted axonemes (Fig. 3 *b*). In each case a single bundle of microtubules, subset 2, slid proximally toward the sperm head relative to microtubule subset 1 (Fig. 3, *arrows*). The advantages of this system of microtubule sliding for measuring rates of sliding were the relatively long length of microtubules that slid (10–40 μm) and the likelihood that sliding resulted from forces between only two sets of microtubules (see reference 37) (i.e., either a single row of both outer and inner arms in intact axonemes or a single row of inner arms in outer arm–depleted axonemes). In 1 mM ATP, subset 2 of outer arm–depleted axonemes slid at 7.86 μm/s ± 3.08 SD (n = 8), and subset 2 of dynein arm intact axonemes slid at 15.95 μm/sec ± 4.67 SD (n = 5).

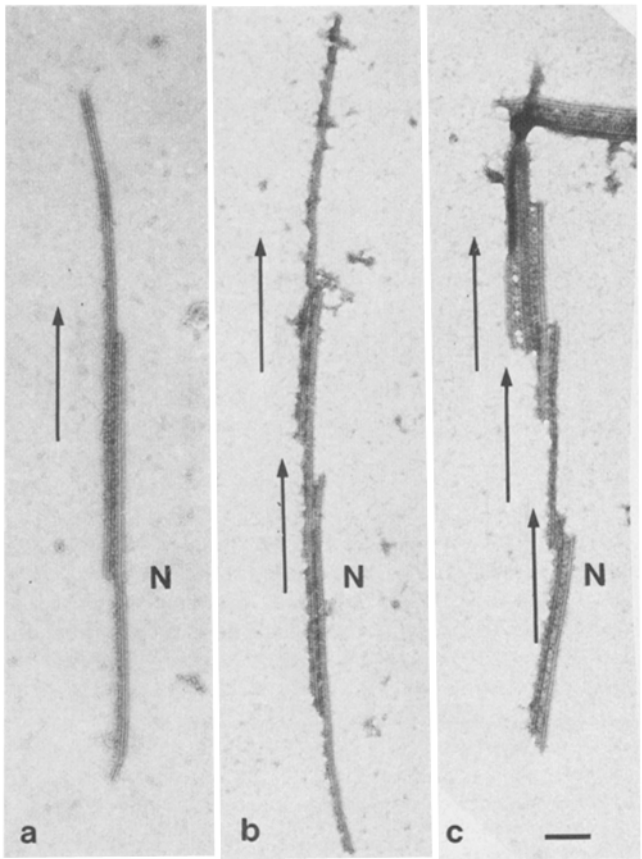

Figure 5. Examples of microtubule sliding illustrating the unique sliding configuration in which doublets have telescoped along their neighbors. In each example, doublet N is equal in length to doublet N+1, etc., and doublet N+1, etc. has slid in a constant direction relative to doublet N. Bar, 0.25 μm.

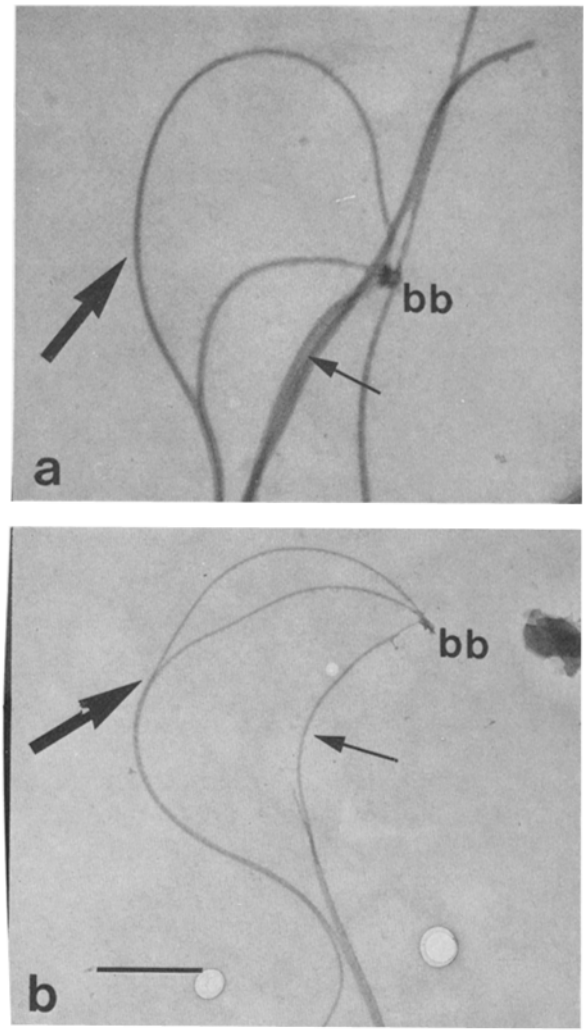

Figure 6. Frequently axonemal fragments, treated with ATP and trypsin, retained the basal body (*bb*), an unequivocal marker of the proximal end of the axoneme. In these examples doublets forming the large loops (*large arrows*) apparently slid in the proximal direction relative to the straighter doublet microtubule groups at the inner edge of the curve (*small arrows*). Analysis of such images revealed that doublet N always slid proximally relative to doublet N+1 (see Fig. 7). Bar, 10 μm.

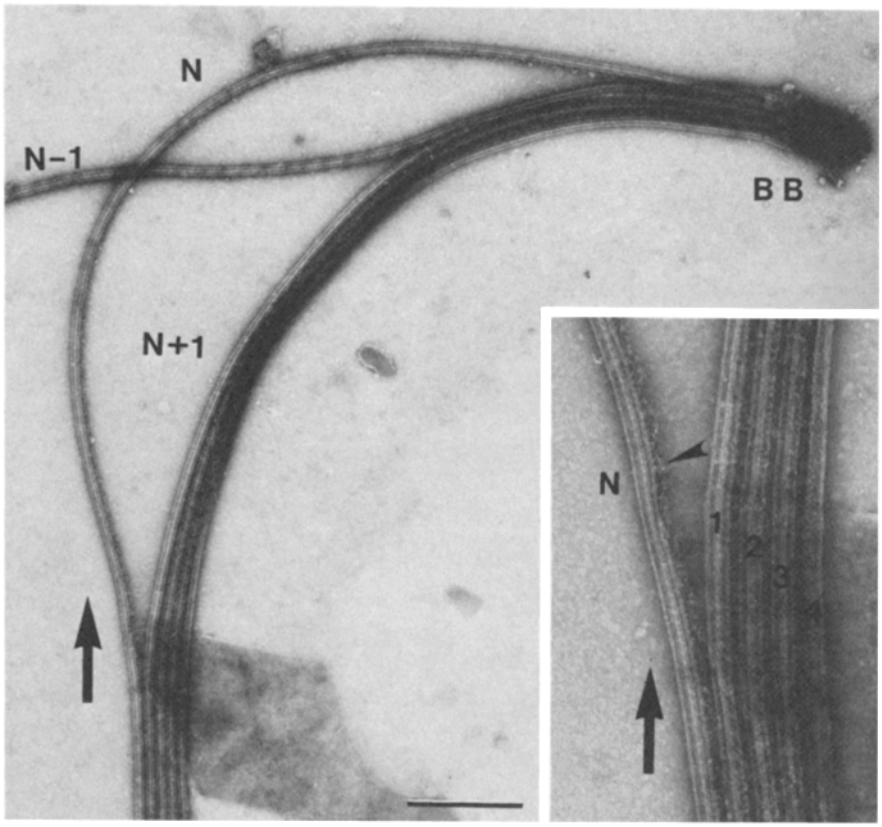

Figure 7. High magnification view of the basal region of an axonemal fragment in which doublet microtubules can be identified and numbered by conventional criteria. In every case examined, doublet N slides in the proximal direction relative to doublet N+1 and forms the basal loop. The inset illustrates negatively stained dynein arms (*arrowhead*) by which doublet N was defined. The morphology of the inner arms was inadequately preserved to unequivocally determine their periodicity or structure. Bar, 0.5 μm.

Directionality of Microtubule Sliding

Homogenization resulted in fracture of the demembranated sperm tails into fragments of various lengths. Light microscopy revealed that treatment with ATP and trypsin produced active microtubule sliding as described previously for intact (45, reviewed in 31) or outer arm–depleted axonemes (21, 31, 54). Addition of ATP alone or trypsin alone did not result in sliding disruption. Axonemes remained intact or splayed out on the glass surface. Buffer control, trypsin- or ATP-treated samples remained either intact or splayed out on the surface of grids viewed by electron microscopy (Fig. 4). However, no intact axonemes remained after treatment with a combination of trypsin and ATP when viewed by electron microscopy and as expected from light microscopic observations. Rather, a unique configuration of telescoping doublet microtubules were seen. These evidently represented the results of microtubule sliding (Fig. 5 and reference 38). Characteristic of such images is that each doublet N, the doublet with the dynein arms projecting to the left in Fig. 5, is equal in length to doublets N+1, N+2, etc. These observations show that the images were not artifacts produced by a fracture or break at the point of overlap. Rather, the translated microtubules were equal in length to the original axonemal fragment before sliding. Also, doublets N+1, N+2, etc. were always displaced in the same direction relative to doublet N (Fig. 5). However, to determine the polarity of sliding it was necessary to identify the distal and proximal directions along any axonemal doublet as well as to identify doublet N (see reference 38). Images such as those of Fig. 5 did not retain unequivocal markers of the distal and proximal directions. Therefore, it was not possible to determine if doublet N+1 slid tipward or baseward relative to doublet N.

Fortuitously, many axonemal fragments were found that retained the basal body, an unequivocal marker of the proximal end of the axoneme (Fig. 6, *bb*). These fragments always had the same configuration, in which bundles of microtubules formed a shallow, centripetal arc (Fig. 6, *small arrows*) and other microtubules formed larger loops on the periphery of the arc (Fig. 6, *large arrows*). These large loops appeared to result from proximal directed microtubule sliding of the doublets of the large loops. Such configurations were never seen in control samples treated with ATP or trypsin alone.

As illustrated at higher resolution in Fig. 7, we found that the proximally translated doublet was always doublet N, relative to the doublets of the arc. In this example doublet numbers can be identified by the presence of dynein arms and residual spoke material (Fig. 7, *inset*). Doublet N formed a basal loop as described in Fig. 6 and slid in the proximal direction relative to doublets N+1, etc. The alternative was that doublet N+1 formed the basal loop and was pushed baseward by doublet N. This was never seen. Evidently doublet N moved in the proximal direction by the power of its own inner row of dynein arms. With careful extensive mapping and analysis of such sliding configurations we never found an exception to this polarity. Doublet N−1 either slid completely off doublet N (Fig. 7) or, in a piggy-back configuration, formed an even larger loop (Fig. 6 *a*). Therefore, the inner row of dynein arms of doublet N generated a net force in a single direction such that doublet N+1 moved tipward, or that doublet N moved baseward relative to doublet N+1.

Discussion

Our goal was to determine the direction of microtubule sliding in axonemes completely devoid of the outer row of dynein arms in order to determine the polarity of force generation of the inner row of dynein arms. Based on electron microscopy, gel electrophoresis, immunoblots, and beat frequency, we are confident that our method efficiently removed only the outer row of arms. This is the first description of successful reactivation of normal motility in outer arm–depleted sperm tail axonemes since the original account by Gibbons and Gibbons (9). In agreement with the earlier results, we found that the inner arms alone generate half the beat frequency (9) and half the microtubule sliding rates (21, 54) of intact axonemes. We conclude, along with others, that the outer dynein arms are not absolutely necessary for motility (9, 25, 30). In accordance with Mitchell and Rosenbaum (30) and based upon the calcium/ATP induction of stationary bends in both intact and outer arm depleted axonemes, we conclude that the outer arms are not required for certain calcium responses. These methods provide a new opportunity for the study of the composition and mechanism of the inner dynein arms and regulation of motility in axonemes devoid of outer arms.

Where outer arms were removed, ATP and trypsin induced microtubule sliding in a single direction, and the inner dynein arms generated force such that the doublet N pushed doublet N+1 tipward (Fig. 8, *a* and *b*). This is the same polarity of microtubule sliding as observed for intact axonemes containing both the inner and outer row of dynein arms (38). Unless trypsin removes the capacity of dyneins to generate active sliding in the opposite direction, all dyneins generate force from the proximal to the distal direction. Therefore, to generate oscillatory bends, all the dynein arms around the radius of the axoneme cannot be simultaneously active. Rather, the inner and outer arms of doublets on one half of the axoneme must be either coordinately active, forming cross-bridges as the axoneme bends in one direction, or coordinately inactive, as the axoneme bends in the opposite direction. Models of ciliary bending based on a single direction of force generation have been described (37, 40, 44, 46, 53). The data presented in this paper provide additional experimental support for this model.

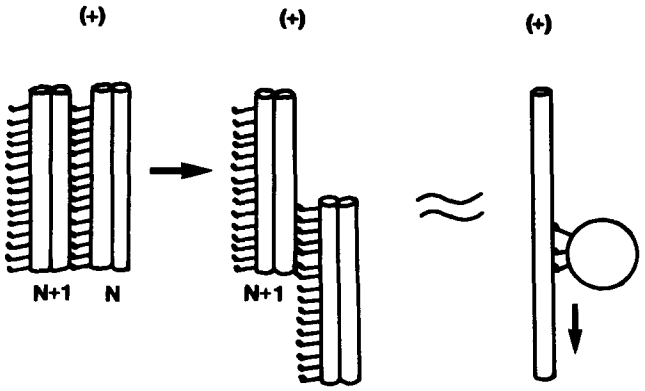

Figure 8. Diagram that summarizes the direction of active microtubule sliding generated by the dynein arms (see also Fig. 8 in ref. 38). The distal end of the microtubules is designated with a plus (+) sign and the proximal end with a minus (−) sign. The doublets are viewed from the inside of the axoneme toward the outside. Doublet N is the doublet with the active arms and doublet N+1 is the adjacent doublet, counting in the direction defined by convention. As illustrated in *a* and *b*, doublet N always slides proximally. More generally, and hypothetically, dynein-mediated motility is toward the minus (−) end of the cytoplasmic microtubule along which dynein, and associated structures, move (*c*).

We only studied axonemes from sea urchin sperm tails in this work. Waveforms vary greatly between cilia and flagella from different cells (12, 40). It is possible in other conditions or in other species that dynein generates force in the opposite direction. However, so far the net direction of relative microtubule sliding is identical for sea urchin sperm tail axonemes, *Tetrahymena* ciliary axonemes (38), and *Chlamydomonas* flagellar axonemes (George Witman, personal communication). To further test the hypothesis that all dyneins generate force with the same polarity, the analysis described here could be applied to axonemes of mutant *Chlamydomonas* flagella devoid of specific dynein components (reviewed in reference 31).

The discovery that all axonemal dyneins generate force with the same directionality may be useful in future identification and definition of cytoplasmic dyneinlike molecules (reviewed in reference 35). Dynein is a polar molecule with functionally distinct domains; the B end undergoes cyclic cross-bridge attachments in contrast to the firmly attached A end (reviewed in references 20 and 24). Given that cytoplasmic organelles have an A end binding site for dynein, such organelles would move toward the minus end of the microtubule track (Fig. 8 *c*, see also reference 39). For example, this would be the retrograde direction along microtubules of the axon in nerve cells (29, 51) or the chromosome-to-pole direction in mitotic spindles (8, 48). Therefore with application of suitable functional assays by which to determine the direction of movement along microtubules of known orientation (see references 15 and 51), and assuming the dynein translocator is firmly associated with the organelle to be translocated, the direction of movement could be added to the criteria used to define cytoplasmic dyneins. For example, a microtubule-associated ATPase translocator has recently been isolated from *Caenorhabditis elegans* that has certain properties in common with dynein but generates force in the same direction as kinesin (28). Therefore, by the criteria we establish, this microtubule translocator would not be defined as dynein.

We thank Gianni Piperno for valuable discussions and the generous gift of the anti-dynein C-241-2. We also thank Cathy Alden for careful preparation of the final manuscript.

This work was supported by National Institutes of Health research grants HD-20497 and Research Career Development Award HD-00553 to W. S. Sale.

Received for publication 31 March 1987, and in revised form 19 May 1987.

References

1. Allen, R. D., and N. S. Allen. 1983. Video-enhanced microscopy with a computer frame memory. *J. Microsc. (Oxf.)*. 129:3–17.
2. Allen, R. D., D. G. Weiss, J. H. Hayden, D. T. Brown, H. Fujiwake, and M. Simpson. 1985. Gliding movement and bidirectional organelle transport along single native microtubules from squid axoplasm: evidence for

an active role of microtubules in cytoplasmic transport. *J. Cell Biol.* 100: 1736–1752.
3. Avolio, J., A. N. Glazzard, M. E. Holwill, and P. Satir. 1986. Structures attached to doublet microtubules of cilia: computer modeling of thin-section and negative-stain stereo images. *Proc. Natl. Acad. Sci. USA.* 83: 4804–4808.
4. Brady, S. T. 1985. A novel brain ATPase with properties expected for the fast axonal transport motor. *Nature (Lond.).* 317:73–75.
5. Brokaw, C. J. 1986. Sperm motility. *Methods Cell Biol.* 27:41–56.
6. Brokaw, C. J., and R. Kamiya. 1987. Bending patterns of Chlamydomonas flagella. IV. Mutants with defects in inner and outer dynein arms indicate differences in arm functions. *Cell Motil. Cytoskeleton.* In press.
7. Euteneuer, U., and J. R. McIntosh. 1981. Polarity of some motility-related microtubules. *Proc. Natl. Acad. Sci. USA.* 78:373–376.
8. Eutenuer, U., and J. R. McIntosh. 1981. Structural polarity of kinetochore microtubules in PtK_1 cells. *J. Cell Biol.* 89:338–345.
9. Gibbons, B. H., and I. R. Gibbons. 1973. The effects of partial extraction of dynein arms on the movement of reactivated sea-urchin sperm. *J. Cell Sci.* 13:337–357.
10. Gibbons, B. H., and I. R. Gibbons. 1979. Relationship between the latent adenosine triphosphatase state of dynein 1 and its ability to recombine functionally with KCl-extracted sea urchin sperm flagella. *J. Biol. Chem.* 254:197–201.
11. Gibbons, B. H., W.-J. Y. Tang, and I. R. Gibbons. 1985. Organic anions stabilize the reactivated motility of sperm flagella and the latency of dynein 1 ATPase activity. *J. Cell Biol.* 101:1281–1287.
12. Gibbons, I. R. 1981. Cilia and flagella of eukaryotes. *J. Cell Biol.* 91: 107s–124s.
13. Gibbons, I. R., and E. Fronk. 1979. A latent adenosine triphosphatase form of dynein 1 from sea urchin sperm flagella. *J. Biol. Chem.* 254:187–196.
14. Gilbert, S., and R. D. Sloboda. 1986. Identification of a MAP2-like ATP-binding protein associated with axoplasmic vesicles that translocate on isolated microtubules. *J. Cell Biol.* 103:947–956.
15. Gilbert, S. P., R. D. Allen, and R. D. Sloboda. 1985. Translocation of vesicles from squid axoplasm on flagellar microtubules. *Nature (Lond.).* 315: 245–248.
16. Goodenough, U. W., B. Gebhardt, V. Memall, D. R. Mitchell, and J. E. Heuser. 1987. High-pressure liquid chromatography fractionation of *Chlamydomonas* dynein extracts and characterization of inner-arm dynein subunits. *J. Mol. Biol.* 194:481–494.
17. Goodenough, U.W., and J. E. Heuser. 1985. Substructure of inner dynein arms, radial spokes, and the central pair/projection complex. *J. Cell Biol.* 100:2008–2018.
18. Goodenough, U. W., and J. E. Heuser. 1985. Outer and inner dynein arms of cilia and flagella. *Cell.* 41:341–342.
19. Gorbsky, G. J., P. J. Sammak, G. G. Borisy. 1987. Chromosomes move poleward in anaphase along stationary microtubules that coordinately disassemble from their kinetochore ends. *J. Cell Biol.* 104:9–18.
20. Haimo, L. T., and R. D. Fenton. 1984. Microtubule crossbridging by Chlamydomonas dynein. *Cell Motil.* 4:371–385.
21. Hata, H., Y. Yano, T. Mohri, T. Miki-Noumura. 1980. ATP driven tubule extrusion from axonemes without outer dynein arms of sea urchin sperm flagella. *J. Cell Sci.* 41:331–340.
22. Huang, B., G. Piperno, and D. J. L. Luck. 1979. Paralyzed flagella mutants of *Chlamydomonas reinhardtii*. *J. Biol. Chem.* 254:3091–3099.
23. Inoue, S. 1981. Cell division and the mitotic spindle. *J. Cell Biol.* 91:131s–147s.
24. Johnson, K. A. 1985. Pathway of the microtubule-dynein ATPase and the structure of dynein: a comparison with actomyosin. *Annu. Rev. Biophys. Chem.* 14:161–188.
25. Kamiya, R., and M. Okamoto. 1985. A mutant of *Chlamydomonas reinhardtii* that lacks the flagellar outer arms but can swim. *J. Cell Sci.* 74: 181–191.
26. Koonce, M. P., and M. Schliwa. 1986. Reactivation of organelle movements along the cytoskeletal framework of a giant freshwater ameba. *J. Cell Biol.* 103:605–612.
27. Kuznetsov, S. A., and V. I. Gelfand. 1986. Bovine brain kinesin is a microtubule-activated ATPase. *Proc. Natl. Acad. Sci. USA.* 83:8530–8534.
28. Lye, J. R., M. E. Porter, J. M. Scholey, and J. R. McIntosh. 1986. Identification of a microtubule-based cytoplasmic motor in the nematode *C. elegans*. *J. Cell Biol.* 103(5, pt. 2):550a. (Abstr.)
29. Miller R. H., and R. J. Lasek. 1985. Cross-bridges mediate anterograde and retrograde vesicle transport along microtubules in squid axoplasm. *J. Cell Biol.* 101:2181–2193.
30. Mitchell, D., and J. L. Rosenbaum. 1985. A motile Chlamydomonas flagellar mutant that lacks outer dynein arms. *J. Cell Biol.* 100:1228–1234.
31. Okagaki, T., and R. Kamiya. 1986. Microtubule sliding in mutant Chlamydomonas axonemes devoid of outer or inner dynein arms. *J. Cell Biol.* 103:1895–1902.
32. Piperno, G. 1984. Monoclonal antibodies to dynein subunits reveal the existence of cytoplasmic antigens in sea urchin egg. *J. Cell Biol.* 98:1842–1850.
33. Piperno, G., and D. J. L. Luck. 1979. Axonemal adenosine triphosphatases from flagella of *Chlamydomonas reinhardtii*. *J. Biol. Chem.* 254:3084–3090.
34. Piperno, G., and D. J. L. Luck. 1981. Inner arm dyneins from flagella of *Chlamydomonas reinhardtii*. *Cell.* 27:331–340.
35. Pratt, M. M. 1986. Homology of egg and flagellar dynein. *J. Biol. Chem.* 261:956–964.
36. Rozdzial, M. M., and L. T. Haimo. 1986. Reactivated melanophore motility: differential regulation and nucleotide requirements of bidirectional pigment granual transport. *J. Cell Biol.* 103:2755–2764.
37. Sale, W. S. 1986. The axonemal axis and Ca^{+2}-induced asymmetry of active microtubule sliding in sea urchin sperm tails. *J. Cell Biol.* 102:2042–2052.
38. Sale, W. S., and P. Satir. 1977. Direction of active sliding of microtubules in Tetrahymena cilia. *Proc. Natl. Acad. Sci. USA.* 74:2045–2059.
39. Satir, P. 1981. Approaches to potential sliding mechanisms of cytoplasmic microtubules. *Cold Spring Harbor Symp. Quant. Biol.* 46(No. 1):285–292.
40. Satir, P. 1985. Switching mechanisms in the control of ciliary motility. *In* Modern Cell Biology. B. Satir, editor. Alan R. Liss, Inc., New York. 1–46.
41. Schnapp, B. J., and T. S. Reese. 1985. New developments in understanding rapid axonal transport. *Trends Neurosci.* 9:155–163.
42. Schnapp, B. J., R. D. Vale, M. P. Sheetz, and T. S. Reese. 1985. The structure of cytoplasmic filaments involved in organelle transport in the squid giant axon. *Cell.* 40:455–462.
43. Scholey, J. M., M. E. Porter, P. M. Grissom, and J. R. McIntosh. 1985. Identification of kinesin in sea urchin eggs, and evidence for its localization in the mitotic spindle. *Nature (Lond.).* 318:483–486.
44. Sugino, K., and Y. Naitoh. 1982. Simulated cross-bridge patterns corresponding to ciliary beating in paramecium. *Nature (Lond.).* 295:609–611.
45. Summers, K., and I. R. Gibbons. 1971. Adenosine triphosphate-induced sliding of tubules in trypsin-treated flagella of sea urchin sperm. *Proc. Natl. Acad. Sci. USA.* 68:3092–3096.
46. Tamm, S. L., and S. Tamm. 1984. Alternate patterns of doublet microtubule sliding in ATP-disintegrated macrocilia of the ctenophore Beroe. *J. Cell Biol.* 99:1364–1371.
47. Tang, W.-J. Y., C. W. Bell, W. S. Sale, and I. R. Gibbons. 1982. Structure of the dynein-1 outer arm in sea urchin sperm flagella. I. Analysis by separation of subunits. *J. Biol. Chem.* 257:508–575.
48. Telzer, B., and L. Haimo. 1981. Decoration of spindle microtubules with dynein: evidence for uniform polarity. *J. Cell Biol.* 89:373–378.
49. Towbin, H., T. Staehelin, and J. Gordon. 1979. Electrophoretic transfer of proteins from polyacrylamide gels to nitrocellulose sheets: procedure and some applications. *Proc. Natl. Acad. Sci. USA.* 76:4350–4354.
50. Vale, R. D., T. S. Reese, and M. P. Sheetz. 1985. Identification of a novel force-generating protein, kinesin, involved in microtubule-based motility. *Cell.* 42:39–50.
51. Vale, R. D., B. J. Schnapp, T. Mitchison, E. Steuer, T. S. Reese, and M. P. Sheetz. 1985. Different axoplasmic proteins generate movement in opposite directions along microtubules in vitro. *Cell.* 43:623–632.
52. Vale, R. D., B. J. Schnapp, T. S. Reese, and M. P. Sheetz. 1985. Organelle, bead and microtubule translocation promoted by soluble factors from the squid giant axon. *Cell.* 40:559–569.
53. Wais-Steider, J., and P. Satir. 1979. Effects of vanadate on gill cilia: switching mechanism in ciliary beat. *J. Supramol. Struct.* 11:339–347.
54. Yano, Y., and T. Miki-Noumura. 1981. Recovery of sliding in arm-depleted flagellar axonemes after recombination with extracted dynein 1. *J. Cell Sci.* 48:223–239.